PERGAMON

International Journal of Heat and Mass Transfer 43 (2000) 2155–2175

International Journal of HEAT and MASS TRANSFER

www.elsevier.com/locate/ijhmt

Thermocapillary effect on drying of a polymer solution under non-uniform radiant heating

Jyh-Jian Chen, Jenn-Der Lin*

Department of Mechanical Engineering, National Chiao Tung University, 1001 Ta Hsueh Road, Hsinchu 30050, Taiwan

Received 20 April 1999; received in revised form 3 September 1999

Abstract

This theoretical investigation analyzes the two-dimensional heat and mass transfer characteristics arising from the non-uniform radiant incidence in polymer solutions whose motion is governed by combined thermocapillary/buoyancy laminar flow. Also considered herein is the evaporation of solvent at solution surface. The effects of various radiation input, external convective parameters, and important physical properties of solutions on the drying characteristics are investigated and results are presented in terms of flow, thermal, and concentration fields, and rate of water removal. In addition, the influence of thermocapillary effect on drying features is also examined. Numerical results indicate that absorbed energy and distribution of the solvent concentration dominate the drying rate. At larger surface tension Reynolds number, more mass concentration can be transferred by thermocapillary flow from the interior region to the surface, which then increases drying rate. Furthermore, removing the solid wall effect reduces the drying time required for a solution film with two sides of symmetric surfaces, which is irradiated by an array of infrared radiant heaters.

1. Introduction

An important physical process in the coating industry is the removal of volatile materials from a coating layer. An improper processing may considerably degrade the quality of products because it is found only in the final manufacturing process. Therefore, understanding the kinetics of heat and mass transfer of a polymer film cast from a polymer/solvent solution is a relevant issue in numerous industrial processes. Among those applications include the drying of paintings, pulps and papers. The drying of a polymer solution plays a crucial role in the manufacture of photographic films, synthetic fibers, adhesives, book coverings, magnetic media and many other kinds of polymeric products. During the drying of wet materials, simultaneous heat and mass transfer occur both inside the medium and in the boundary layer of the drying agent. Some researchers have measured mass diffusion coefficients and applied them to predict the drying characteristics of polymeric coatings under convective heating [1,2]. Vrentas and Vrentas [3] derived a set of equations to describe the two-dimensional heat and mass transfer and film shrinkage in the convective drying of polymer films. However, their work did not contain any numerical results. Guerrier et al. [4] considered the drying kinetics of a polymer film cast from a polymer/solvent solution. They also examined how convective heat transfer coefficients and physicochemical properties of the

* Corresponding author. Tel.: +886-3-5727-923; fax: +886-3-5714-732.

E-mail address: jdlin@cc.nctu.edu.tw (J.-D. Lin).

0017-9310/00/$ - see front matter
PII: S0017-9310(99)00277-X

Nomenclature

A aspect ratio (y_0/x_0)
Bi Biot number for heat transfer (hy_0/k)
Bi_m Biot number for mass transfer ($h_m y_0/D_0$)
c mass fraction of water
c_p specific heat
C dimensionless mass fractions of water (c/c_0)
Ca capillary number ($\gamma T_0/\sigma_0$)
D mass diffusivity
$\hat{D}$ dimensionless mass diffusion coefficient (D/D_0)
g gravitational force per unit mass
Gr Grashof number for heat transfer ($g\beta_T T_0 y_0^3/\nu_0^2$)
Gr_m Grashof number for mass transfer ($g\beta_c c_0 y_0^3/\nu_0^2$)
h convective heat transfer coefficient
h_m convective mass transfer coefficient
Ja Jacob number ($c_p T_0/\gamma_A$)
k thermal conductivity
P dimensionless pressure ($\frac{p}{\gamma T_0/y_0}$)
Pr Prandtl number (ν_0/α_0)
Re Reynolds number ($U_0 y_0/\nu_0$)
s height of free surface
$\bar{s}$ standard deviation of the Gaussian distribution
S dimensionless geometric thickness of solution layer (s/y_0)
Sc Schmidt number (ν_0/D_0)
t time
T temperature
u horizontal velocity component
U dimensionless horizontal velocity component
v vertical velocity component
V dimensionless vertical velocity component
x, y distance coordinates
y_0 initial height of free surface

Greek symbols
α thermal diffusivity
$\hat{\alpha}$ dimensionless thermal diffusivity (α/α_0)
β_T thermal expansion coefficient
β_c a quantity that indicates the dependence of density with composition
γ temperature coefficient of surface tension
γ_A latent heat of water
μ dynamic viscosity
$\hat{\mu}$ dimensionless dynamic viscosity (μ/μ_0)
ν kinematic viscosity
θ dimensionless temperature
ξ, η dimensionless distance coordinates
ρ total density
$\mathring{\rho}$ density
σ surface tension
ψ dimensionless radiative intensity or dimensionless stream function
ζ^* dimensionless time

Subscript
0 initial value

solution affect convective drying. Drying by high intense thermal radiation, instead of conventional hot air, has been used in a number of fields to optimize the process and reduce energy consumption. Fundamental studies relating to the applications of infrared radiation in drying have received considerable attention in recent years [5,6]. In a continuous infrared dryer, the electric infrared sources may be placed in several modules, situated transversely with respect to the moving web. And each module may support more than one emitter which consists of heating elements inside quartz tubes [7]. A gas-fired infrared heater composed of several emitter modules, arranged in a specific configuration, may also be used [8]. In drying of wet bed, drying samples were contained in an insulated sample holder [9]. Applications of infrared radiation have the following merits: easy and rapid thermal control, clean working environment, and straight forward heat transfer. However, poorly chosen drying conditions cause unwanted internal temperature gradients, phase separations, and various stress-related failures or defects [10]. During the drying processes, non-uniform heating can result in a temperature gradient on the surface of heated objects. For liquid film, the thermocapillary effect induced by a non-uniform temperature may result in local thinning, and even a dimpling surface or rupture of film [11,12], ultimately deteriorating the quality of dried products. Experimental results also demonstrate that drying paint films often display a steady, cellular, circulatory flow of the same type as observed in Benard cells [13]; thermocapillarity may influence the heat and mass transfer characteristics during drying.

A variety of problems in hydrodynamics and in the theory of convective heat and mass transfer in two-phase systems with mobile interphase boundaries (liquid–liquid or liquid–gas) reveal the so called capillary phenomena, i.e., phenomena caused by the existence of surface tension on the interface boundary. These phenomena are due to intermolecular attractions

of non-vanishing resultant at the interphase boundary. Capillary phenomena may occur in two cases: (a) when the surface of phase separation is considerably curved, and (b) when the surface tension varies from point to point. Since surface tension is a function of temperature, composition, and electrical potential, gradients of any one of these or combinations of them, lead to surface-tension gradients. In both cases, forces arise near the boundary that change the nature of the motion in each phase or induce motion that is originally absent. These flows are analogous to conventional convection and are called thermocapillary, diffusocapillary, or thermoelectric flows, according to their respective causes, viz. temperature, concentration, or electric potential gradients. Capillary flows play a dominant role in many important engineering applications. For example, many important fluid flow patterns are found in lubrication, electrochemical plating, corrosion, coating, polymer technology, separation processes, metal and glass manufacturing processes, crystal growth and aerospace technology. If the surface tension at the free surface between a liquid and a gas phase is not uniform, a tangential force is exerted whose magnitude is determined by the surface tension gradient. If the latter is subsequently determined by the spatial variation in surface temperature, the induced hydrodynamics phenomenon is known as thermocapillary motion or Marangoni convection. The thermocapillary flow is induced from the balance on the interface of the jump in bulk shear stress and the surface tension gradient along the interface. This interfacial stress is transmitted to the bulk by viscous forces. Consequently, a thermocapillary flow is induced from warm to cold regions of the surface, and the height of the cold region may change following the local value of the surface tension. Flows driven by thermally induced surface tension gradients have been examined due to their practical applications and complex flow patterns. They were recognized as an important aspect of several areas of technology either in low gravity containerless materials processing as a dominant source of fluid motion, or in conventional crystal growth and welding processes as a contributing factor. Thus, the thermocapillary phenomena must be elucidated in order to understand their effects on the flow characteristics and/or to improve the product quality. Many studies in recent decades have analyzed the thermocapillary flows in a cavity. Hadid and Roux [14] thoroughly reviewed how thermocapillary- and/or buoyancy-driven forces affect flows in a horizontal layer or open cavities; they also analyzed in detail how the flow regime in shallow cavities of large aspect ratio is related to the relative strength of the two forces. While measuring the surface tension of the absorbing solution, Hozawa et al. [15] experimentally and numerically demonstrated the Marangoni convection during steam absorption into LiBr solution. According to their results, liquid volume did not change during steam absorption. Ahmed and Ball [16] performed a detailed survey of the early experimental and analytical studies of the thermocapillary convection problem. They also developed a Chebyshev collocation spectral method to investigate thermocapillary- and/or buoyancy-induced flow within a deformable free surface.

Most investigations included systems that analyzed one-dimensional heat and mass transfer under drying [1,2,5,6]. While considering the two-dimensional problem of polymer solution drying, those investigations neglected the thermocapillary effect induced by a non-uniform temperature [3]. Or the liquid volume was assumed to maintain a constant value in Marangoni convection during steam absorption [15]. To our knowledge, no previous effort has been made to study two-dimensional thermocapillary motion in a polymer solution film that is dried under radiation and convection heat. The drying process for coatings is a complex problem involving heat, mass, and momentum transfer in polymeric solutions. An appropriate model of this process must take into account phenomena including the flow of polymer films, convective and/or radiative heating of the coating, evaporation of the solvent from the coating surface, evaporative cooling, mass transfer resistances in the vapor and polymer phases, and film shrinkage. In this investigation, the governing equations are recast in terms of a vorticity/stream function formulation together with a coordinate transformation. The transient Navier–Stokes, energy and

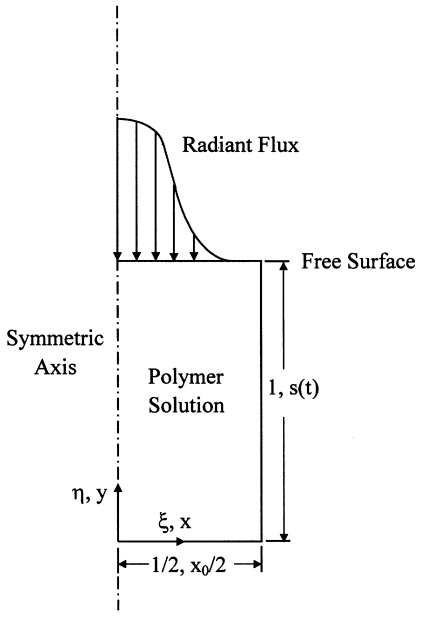

Fig. 1. Basic configuration and coordinate system.

mass transfer equations are solved for a solution film with a top free surface. The finite difference method is used to study buoyant thermocapillary convection of polymer solution in drying process under radiation heat. The input power distribution due to the heat source is assumed to be Gaussian. As assumed herein, the polymer solution is optically thick and the thermal radiation interacting with the solution is only a boundary phenomenon at the free surface. The influences of thermocapillary effect on drying features is expressed in terms of the surface tension Reynolds number. This work also describes the extent to which various radiation input, external convection parameters, and physical properties of polymer solution during the drying processes affect drying characteristics in terms of the rate of solvent removal and stream function, temperature, and concentration distributions. Particular emphasis is placed on qualitative analysis of the physical phenomena, which will benefit the study of material processing in industrial applications.

2. Mathematical model

Fig. 1 schematically depicts the basic configuration and coordinate system for the analysis. The physical problem is a polymer solution film irradiated by an infrared radiant heater, where x_0 is the spacing between two walls which confine the solution or the spacing between two surfaces of symmetry. The physical domain is a two-dimensional rectangular zone having a length of $x_0/2$ and height of $s(t)$ due to the symmetry of the problem and the left surface is a symmetric surface. In addition, y_0 is initial height of solution, i.e., equal to $s(0)$. The bottom surface of the domain is a solid, rigid and impermeable wall, and an adiabatic condition is assumed. The top surface of the domain is the free surface. Although the surface deformation is neglected, the height of the solution changes with time due to solvent evaporation. The input power distribution due to the heat source is assumed to be Gaussian. It is further assumed that the polymer solution is optically thick since for polymer solutions the spectral absorption coefficient is greater than 10^4 m^{-1} in the wavelength range of 2.5–20 μm and thus, the thermal radiation interaction with the solution is only a boundary phenomenon at the free surface. The origin of the coordinate frame of reference is at the lower left corner of the physical domain. The vertical symmetric surface is perfectly aligned in the direction of the gravitational force. The problem involves two driving forces: the thermocapillary acting on the upper surface of the fluid and the buoyancy acting as a body force in the bulk. The bulk fluid flow is influenced by the thermocapillarity associated with the temperature gradient along the free surface and by the buoyancy due to density variations that are primarily near the vertical walls.

The equations to be solved are the continuity equation, the Navier–Stokes equations, and the energy and mass transfer equations along with the appropriate boundary conditions. The following assumptions have been adopted to obtain a proper mathematical formulation of this problem.

1. Fluid flow is Newtonian, incompressible, and laminar.
2. The thermophysical properties of the liquid, such as the viscosity, thermal diffusivity, and mass diffusion coefficient are dependent on the local liquid density and vary with the composition of solution.
3. Gravity is the only external body force, and there are no internal heat sources.
4. The Boussinesq approximation for density variation is valid. And the variations in density are neglected everywhere except in the gravity term. The dependence of density on temperature and concentration can be expressed as

$$\rho = \rho\left[1 - \beta_T(T - T_0) - \beta_c(c - c_0)\right] \tag{1}$$

   where β_T is the thermal expansion coefficient of the fluid, β_c is a quantity that indicates the dependence of the density variation with composition.
5. Surface tension varies linearly with temperature. The dependence of surface tension on temperature can be generally expressed as

$$\sigma = \sigma_0\left[1 - \gamma(T - T_0)\right] \tag{2}$$

   It is assumed that γ, the temperature coefficient of surface tension, is a small positively valued constant indicating that flow will be enhanced in direction of decreasing temperature. Moreover, we assume that the surface tension remains constant everywhere except in the boundary condition for shear stress continuity at the free surface.
6. Both the compression work and viscous dissipation are negligible.

The variables involving length, velocity, temperature, pressure, concentration, and time have been scaled using y_0, α_0/y_0, T_0, $\rho_0(\alpha_0/y_0)^2$, c_0, and y_0^2/α_0, respectively. Aspect ratio A is defined as y_0/x_0. Due to the moving boundary effect, another set of coordinates (ξ, η) have been defined with $\xi = Ax/y_0$ and $\eta = y/s(t)$. These coordinates specify the computational fixed domain. Under the above conditions, the equations are given below in non-dimensional form [17].

$$A\frac{\partial U}{\partial \xi} + \frac{1}{S}\frac{\partial V}{\partial \eta} = 0 \tag{3}$$

$$\frac{\partial U}{\partial \zeta^*}+\frac{\mathrm{d}S}{\mathrm{d}\zeta^*}\frac{\partial U}{\partial \eta}+UA\frac{\partial U}{\partial \xi}+\frac{V}{S}\frac{\partial U}{\partial \eta}$$
$$=-APr\frac{\partial P}{\partial \xi}+Pr\left\{A^2\frac{\partial}{\partial \xi}\left(2\hat{\mu}\frac{\partial U}{\partial \xi}\right)+\frac{1}{S}\frac{\partial}{\partial \eta}\left[\hat{\mu}\left(A\frac{\partial V}{\partial \xi}+\frac{1}{S}\frac{\partial U}{\partial \eta}\right)\right]\right\} \quad (4)$$

$$\frac{\partial V}{\partial \zeta^*}+\frac{\mathrm{d}S}{\mathrm{d}\zeta^*}\frac{\partial V}{\partial \eta}+UA\frac{\partial V}{\partial \xi}+\frac{V}{S}\frac{\partial V}{\partial \eta}$$
$$=-\frac{Pr}{S}\frac{\partial P}{\partial \eta}+Pr\left\{A\frac{\partial}{\partial \xi}\left[\hat{\mu}\left(A\frac{\partial V}{\partial \xi}+\frac{1}{S}\frac{\partial U}{\partial \eta}\right)\right]+\frac{1}{S^2}\frac{\partial}{\partial \eta}\left(2\hat{\mu}\frac{\partial V}{\partial \eta}\right)\right\}+Pr^2Gr(\theta-1)+Pr^2Gr_{\mathrm{m}}(C-1) \quad (5)$$

$$\frac{\partial \theta}{\partial \zeta^*}+\frac{\mathrm{d}S}{\mathrm{d}\zeta^*}\frac{\partial \theta}{\partial \eta}+UA\frac{\partial \theta}{\partial \xi}+\frac{V}{S}\frac{\partial \theta}{\partial \eta}$$
$$=\left\{A^2\frac{\partial}{\partial \xi}\left(\hat{\alpha}\frac{\partial \theta}{\partial \xi}\right)+\frac{1}{S^2}\frac{\partial}{\partial \eta}\left(\hat{\alpha}\frac{\partial \theta}{\partial \eta}\right)\right\} \quad (6)$$

$$\frac{\partial C}{\partial \zeta^*}+\frac{\mathrm{d}S}{\mathrm{d}\zeta^*}\frac{\partial C}{\partial \eta}+UA\frac{\partial C}{\partial \xi}+\frac{V}{S}\frac{\partial C}{\partial \eta}$$
$$=\frac{Pr}{Sc}\left\{A^2\frac{\partial}{\partial \xi}\left(\hat{D}\frac{\partial C}{\partial \xi}\right)+\frac{1}{S^2}\frac{\partial}{\partial \eta}\left(\hat{D}\frac{\partial C}{\partial \eta}\right)\right\}. \quad (7)$$

Some parameters appear in the nondimensional form of the equations. These are the Grashof number Gr, which accounts for the ratio of buoyancy to viscous forces, and the Prandtl number Pr, which shows the relative importance of diffusion of vorticity to that of heat. The Schmidt number Sc is the ratio of the momentum and mass diffusivities. The Prandtl, Grashof, and Schmidt numbers are defined, respectively, as

$$Pr=\frac{\nu_0}{\alpha_0},\quad Gr=\frac{g\beta_T T_0 y_0^3}{\nu_0^2},\quad \text{and}\quad Sc=\frac{\nu_0}{D_0}$$

In the present problem, it is convenient to write the Navier–Stokes equations in the vorticity-stream function form rather than in the primitive form. These equations in the primitive variables demand the specification of boundary conditions on pressure. Such a specification is difficult to make in this problem, and hence, the vorticity-stream function form of these equations is generally preferred. Thus, the original set of three equations, Eqs. (3)–(5), has been reduced to two equations governing the vorticity and stream function. By eliminating the pressure, the dimensionless governing equations for the two-dimensional motion of the liquid are

$$\frac{\partial \omega}{\partial \zeta^*}+\frac{\mathrm{d}S}{\mathrm{d}\zeta^*}\frac{\partial \omega}{\partial \eta}+\frac{A}{S}\frac{\partial \psi}{\partial \eta}\frac{\partial \omega}{\partial \xi}-\frac{A}{S}\frac{\partial \psi}{\partial \xi}\frac{\partial \omega}{\partial \eta}$$
$$=Pr\left[\hat{\mu}\left(A^2\frac{\partial^2\omega}{\partial \xi^2}+\frac{1}{S^2}\frac{\partial^2\omega}{\partial \eta^2}\right)\right]-\left(\frac{1}{S^2}\frac{\partial^2\psi}{\partial \xi^2}-A^2\frac{\partial^2\psi}{\partial \eta^2}\right)\left(\frac{1}{S^2}\frac{\partial^2\hat{\mu}}{\partial \xi^2}-A^2\frac{\partial^2\hat{\mu}}{\partial \eta^2}\right)$$
$$-4\frac{A}{S}\frac{\partial^2\psi}{\partial \xi\partial \eta}\frac{\partial^2\hat{\mu}}{\partial \xi\partial \eta}+\left[2\left(A^2\frac{\partial \hat{\mu}}{\partial \xi}\frac{\partial \omega}{\partial \xi}+\frac{1}{S^2}\frac{\partial \hat{\mu}}{\partial \eta}\frac{\partial \omega}{\partial \eta}\right)\right]+APr^2Gr\theta_\xi+APr^2Gr_{\mathrm{m}}C_\xi, \quad (8)$$

$$-\omega=A^2\frac{\partial^2\psi}{\partial \xi^2}+\frac{1}{S^2}\frac{\partial^2\psi}{\partial \eta^2}. \quad (9)$$

Here, the stream function ψ and the vorticity ω are defined in terms of the velocities U and V as

$$U=\frac{1}{S}\frac{\partial \psi}{\partial \eta}, \quad (10)$$

$$V=-A\frac{\partial \psi}{\partial \xi}, \quad (11)$$

and

$$\omega=A\frac{\partial V}{\partial \xi}-\frac{1}{S}\frac{\partial U}{\partial \eta}. \quad (12)$$

Derivatives of $\hat{D}$, $\hat{\alpha}$ and $\hat{\mu}$ with respect to spatial coordinates occur in the above expressions so as to take into account the effect of composition variation in the system. The non-slip and non-penetration conditions usually encounter at solid surfaces. The initial and boundary conditions are thus given as

$$\omega=0,\quad \theta=1,\quad C=1,\quad \text{at } \zeta=0.$$

$$\omega=0,\quad \psi=0,\quad \frac{\partial \theta}{\partial \xi}=\frac{\partial C}{\partial \xi}=0\quad \text{at } \xi=0. \quad (13)$$

$$\omega=A\frac{\partial V}{\partial \xi},\quad \psi=0,\quad \frac{\partial \theta}{\partial \xi}=\frac{\partial C}{\partial \xi}=0,\quad \text{at } \xi=\frac{1}{2}. \quad (14a)$$

or

$$\omega = 0, \quad \psi = 0, \quad \frac{\partial \theta}{\partial \xi} = \frac{\partial C}{\partial \xi} = 0, \quad \text{at} \quad \xi = \frac{1}{2}. \tag{14b}$$

$$\omega = -\frac{1}{S}\frac{\partial U}{\partial \eta}, \quad \psi = 0, \frac{\partial \theta}{\partial \eta} = \frac{\partial C}{\partial \eta} = 0, \quad \text{at}\, \eta = 0. \tag{15}$$

Eq. (14a) applies for the polymer solution film, which is confined by solid walls and is irradiated by an infrared radiant heater, with x_0 as the spacing between two walls which confine the solution. Eq. (14b) applies as a polymer solution film is irradiated by an array of infrared radiant heaters, and surface of symmetry exists between every two adjacent heaters of spacing x_0.

The boundary conditions at the free surface $S(\zeta)$ are obtained from the tangential stress balance and the heat and mass transfer balances, and are expressed as

$$\psi = 0, \tag{16a}$$

$$\omega = ARePr\frac{\partial \theta}{\partial \xi}, \tag{16b}$$

$$\frac{k}{k_0}\frac{\partial \theta}{\partial \eta} = S\left[- Bi(\theta - \theta_{\text{out}}) + \frac{\mathrm{d}S}{\mathrm{d}\zeta^*}\frac{PrRe}{Ja} + Q_{\text{in}}(\xi)\right], \tag{16c}$$

$$\hat{D}\frac{\partial C}{\partial \eta} = -SBi_{\text{m}}(C - C_{\text{out}}). \tag{16d}$$

The surface tension Reynolds number, $Re = U_0 y_0/\nu_0$, signifies the importance of surface tension relative to viscous force, and the reference velocity U_0, which is driven by the gradient of surface tension, is expressed as

$$U_0 = \frac{\gamma T_0}{\mu}.$$

Ja is the Jacob number, which is the ratio of sensible to latent energy absorbed during liquid–vapor phase change, and is expressed as

$$Ja = \frac{c_{\text{p}} T_0}{\gamma_{\text{A}}}$$

with γ_{A} the latent heat of solvent at the evaporation temperature. The stress balances at the interface in the tangential directions are given by Eqs. (16a) and (16b) and reveal that temperature gradients along the free surface produce surface tension, and that this force drives the flow motion, that is, the thermocapillary convection. The jump in the shear stress equals the surface-tension gradient along the interface. Herein, it is assumed that this surface is nondeformable, but can allow the circulation of the fluid along the ξ direction. Eq. (16b) expresses the equilibrium condition of the surface shear stresses in the ξ direction (the direction along which thermocapillary action takes place). The capillary number Ca is given by

$$Ca = \frac{\gamma T_0}{\sigma_0},$$

which, in this study, tends to be zero, so that the free surface can be assumed to remain flat. The capillary number measures the degree of deformation of the free surface. Thus, as $Ca \to 0$, only very small variations in σ_0 and the surface deformation are allowed, which imply that the surface tension is very large and the free surface remains perfectly flat. Eq. (16c) specifies that the free surface is also in thermal equilibrium with respect to the surrounding environment. The Biot number Bi measures the heat transport between the gas and the liquid phases, and the mass transfer Biot number Bi_{m} measures the ratio of the internal species transfer resistance to the boundary layer species transfer resistance. The input power distribution due to the heat source is assumed to be Gaussian and absorbed at the free surface, and is expressed as

$$Q(\xi) = \frac{Q_0}{\bar{s}\sqrt{2\pi}}\mathrm{e}^{-1/2\left[(\xi - 0.5)/\bar{s}\right]^2}, \tag{17}$$

where Q_0 is the density of the input power and the parameter $\bar{s}$ is the standard deviation of the distribution. As assumed herein, about 99% of the input power lies in the range $0 < \xi < 2.58\bar{s}$. While assuming that the liquid is incompressible, the total liquid height is the original liquid height minus the volume of the drying liquid per area,

$$S(\zeta^*) = S(0) - \int_0^{\zeta^*}\int_0^{1/2} Bi_{\text{m}}(C - C_{\text{out}})\,\mathrm{d}\xi\,\mathrm{d}\zeta'. \tag{18}$$

3. Numerical analysis

Herein, the governing equations of the flow field are recast in terms of a vorticity-stream function formulation together with a coordinate transformation. The latter allows a free boundary to coincide with a coordinate line (or surface) without the need to interpolate grid space. The dimensionless governing equations subject to the initial and boundary conditions constitute a highly nonlinear and coupled system. These equations must be solved appropriately to determine the flow structure, the thermal field, and the concentration field, as well as their temporal evolution. A finite difference method is used to solve the problem and the discrete form of the system is constructed. The time derivatives are forward-differenced, while the derivatives with respect to spatial coordinates are finite-differenced, based on a second-order central-differencing scheme.

The present study adopts the Alternative Direction Implicit (ADI) method to tackle the task at hand. A block tridiagonal matrix inversion algorithm (Thomas algorithm) is employed for the finite-difference form of equations.

A complete solution of the flow, temperature, and concentration fields can be obtained by assigning a specific height to the free surface. A boundary-fitted (orthogonal) coordinate system is found to deal with the moving boundary problem, and this system has coordinate lines coinciding with the surface boundaries. In the present approach, the method of Thompson et al. [18] was employed to transform the physical plane into a rectangular computational domain, where the free surface is selected as a boundary in the computational domain. The parametric relations map the physical $(x,\ y)$ coordinates onto the computational (ξ, η) coordinates. Herein, we let $\xi = Ax/y_0$ and $\eta = y/s(t)$. The time derivative term in the transformed plane can be described as

$$\left.\frac{\partial f}{\partial \zeta^*}\right|_{\text{physical}} = \left.\frac{\partial f}{\partial \zeta^*}\right|_{\text{transformed}} + \frac{\mathrm{d}\eta}{\mathrm{d}\zeta^*}\frac{\partial f}{\partial \eta}. \tag{19}$$

Notably, in the transformed expression for the time derivatives, all derivatives are taken at the fixed grid points in the transformed plane. The movement of the grid in the physical plane is reflected only through the rates of change of η at the fixed grid points in the transformed plane.

The numerical calculation solves the momentum, energy, and mass transfer equations with moving boundary effect. At each time increment, height of free surface is first assumed and the nodal values of temperature and mass fraction are solved. The parameters such as drying rate, thickness of solution, and stream functions, which appear in the coefficients of the finite difference equation, are initially evaluated with the use of the values obtained at the previous time step. The solution of the finite-difference form of the vorticity equation gives the value of vorticity at interior points for the specified value of wall vorticity. The new values of vorticity at interior points can now be used to find the new value of the stream function, by solving the finite-difference form of the stream function equation. The entire cycle is repeated until the maximum relative error of stream function at each nodal point is within 0.1%. The new values of stream functions at the interior points enable us to obtain the new values of wall vorticities. If convergent solutions are not attained, the newly calculated variables are used to update the parameters for the next iteration. The finite difference forms of the energy, mass transfer, and vorticity equations are now solved using the accurate value of stream function obtained from the previous step. Once the convergence is found according to a prescribed condition (in the present study, the prescribed condition is that the maximum relative errors of temperature, mass fraction, vorticity, and concentration are less than 10^{-3}), the volume of the drying liquid per area is calculated and the height of free surface is checked. This procedure is then carried out repeatedly along the time axis. The detailed numerical computational procedure is shown in Fig. 2.

Owing to the thermocapillary effect, large temperature and velocity gradients exist near the free surface. Based on previous numerical analysis, a non-uniform grid system is adopted, which continually increases the grid space by 3%, progressively from the free surface

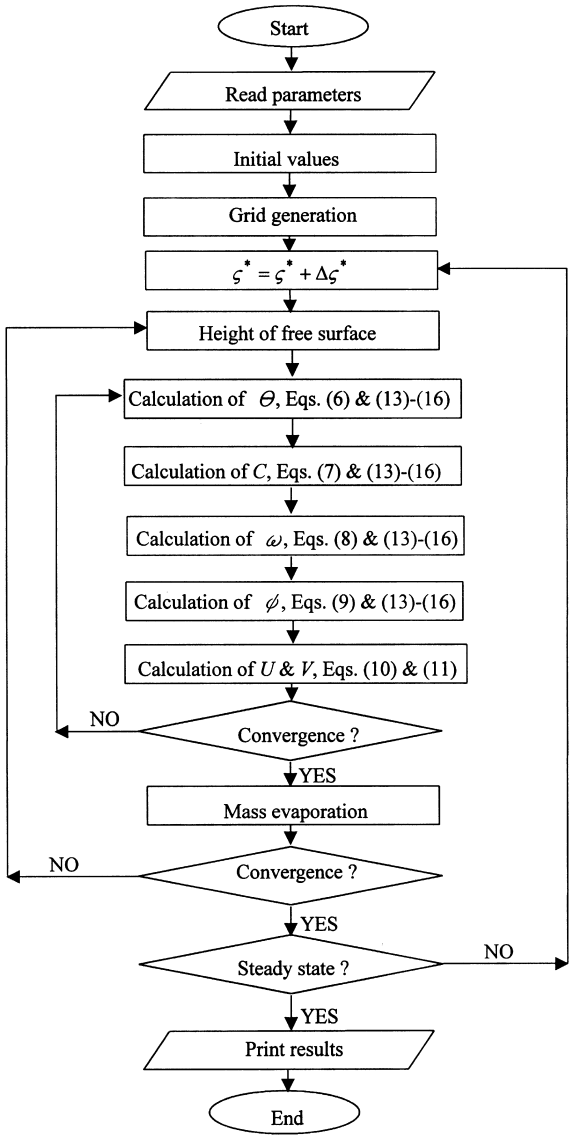

Fig. 2. Computational flow chart.

boundary to the bottom of the domain. The grids used are non-uniform to increase resolution in regions of higher gradients. To determine the proper number of grid points, calculations were performed using different grid points. The effect of grid size has been examined by comparing the results obtained with various non-uniform grid systems. The solution can be confirmed using measures that are invariant to mesh refinement. The non-uniform 51×51 grids are adopted in the general case of the present numerical computation, and is necessary to ensure a grid independent solution. Further reducing the grid spacing does not yield significant differences. The numerical calculations described in the present study are performed in double-precision arithmetic on National Chiao Tung University HP735 workstations.

4. Results and discussion

This study focuses on the influence of various parameters on the drying rate, flow field, and heat transfer in the physical problem. Closely examining the pattern of stream function, temperature, and concentration contours for various radiation input and external convective parameters and physical properties of the polymer solution should reveal the nature of thermocapillary flow during drying. The polymer solution and ambient air are initially at room temperature, which is normalized to 1.0. The Jacob number associated with the simulations is 5.0 and Gr_m is equal to 300. The initial thickness of the solution is 2.5×10^{-3} m with initial concentration $C_0 = 90\%$ by weight. Aspect ratio A is equal to 2.0. The parameters of above values are used if not further specified. The physical properties of water and PVA are tabulated in Table 1.

Figs. 3 and 4 respectively show the results of polymer solution drying with radiation input $Q_{in} = 10$ and 5 at $Re = 10^4$, $Pr = 10$, $Sc = 10^4$, $Gr = 300$, $Bi = 100$ and $Bi_m = 300$. The predicted stream function (upper portion), temperature (central portion), and concentration (bottom portion) contours of the solution at various times are presented. Corresponding results are listed from left to right for $\zeta^* = 50$, 100, 150, and 200, respectively. Owing to the evaporation of solvent, the boundary moves and the thickness of the polymer solution changes. The η in the figures represents the location normalized to the thickness of the solution layer, and the solution surface is located at $\eta = 1.0$. With respect to the drying mechanism in the heating process, the magnitude of heat flux at the left-hand side of free surface is larger than anywhere else in the domain and the isotherms close together. In addition, the fluid temperature at the left side of the free surface is hotter than at the right side. Thus, the surface tension of the fluid near the left side of the free surface is lower than that near the right side. Owing to the surface tension gradient along the free surface, thermocapillary forces cause a shear force in the interior fluid, and the flow pattern consists of a main cell configuration at the upper region. Interestingly, the thermocapillary convection flow develops quite rapidly after starting the heating process. The global structure of the flow does not vary substantially with time, although its intensity is under variation. Thus, the fluid is drawn along the surface from the left side to the right, that is, rising along the left (hot) symmetric surface and sinking along the right (cold) solid surface of the domain. The shear stress caused by thermocapillary phenomena is transmitted into the interior of the fluid, due to the viscous action of the fluid. A short time after starting the heating process, there is a pronounced temperature gradient over the entire free surface. Such behavior is the cause of the high level of stream function. This is borne out by the fact that the contours of stream function are initially packed closer to the free surface and to the right solid surface, indicating higher velocities of the fluid in that region. For

Table 1
The physical properties of water and PVA[a]

Properties	PVA[b]	Water[c]
Thermal conductivity, k (W/m/K)	0.169	0.604
Specific heat, c_p (J/kg/K)	1670	4179
Thermal expansion coefficient, β_T (1/K)	9.5×10^{-5}	2.761×10^{-4}
Surface tension gradient, γ (kg/s^2/K)	4×10^{-4}	2×10^{-4}
Surface tension, σ_0(kg/s^2)	0.06	0.0717
Dynamic viscosity, μ_0(kg/m/s)	1.1	9.8×10^{-4}
Density, $\mathring{\rho}$(kg/m^3)	1110	997.4

[a] The reference temperature is 300 K.
[b] Blomstrom [19].
[c] Holman [20].

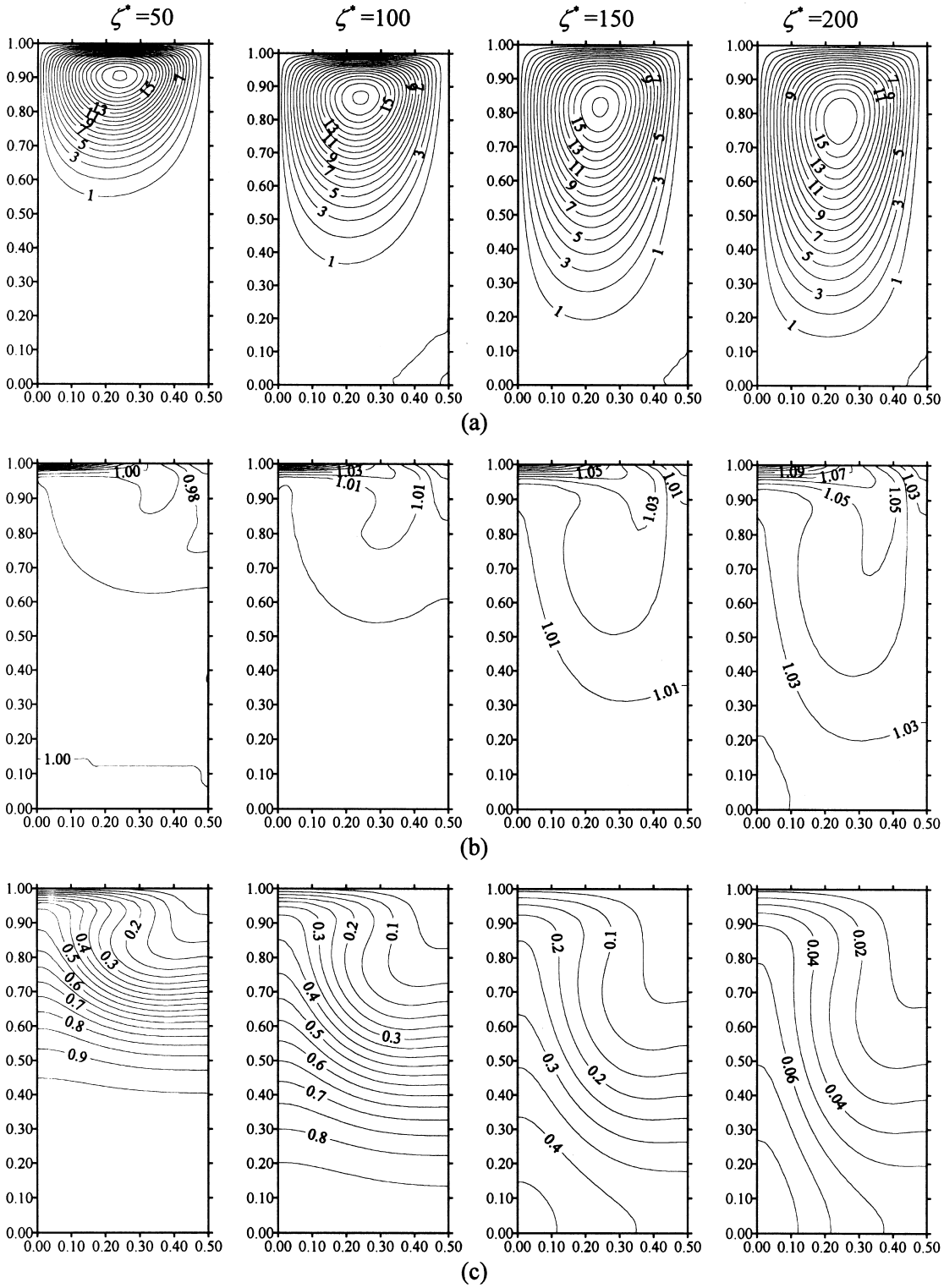

Fig. 3. The predicted stream function, temperature, and concentration contours of the solution in (ξ, η) domain at $\zeta^* = 50$, 100, 150, 200 with $Q_{in} = 10$, $Re = 10^4$, $Pr = 10$, $Sc = 10^4$, $Gr = 300$, $Bi = 100$, and $Bi_m = 300$.

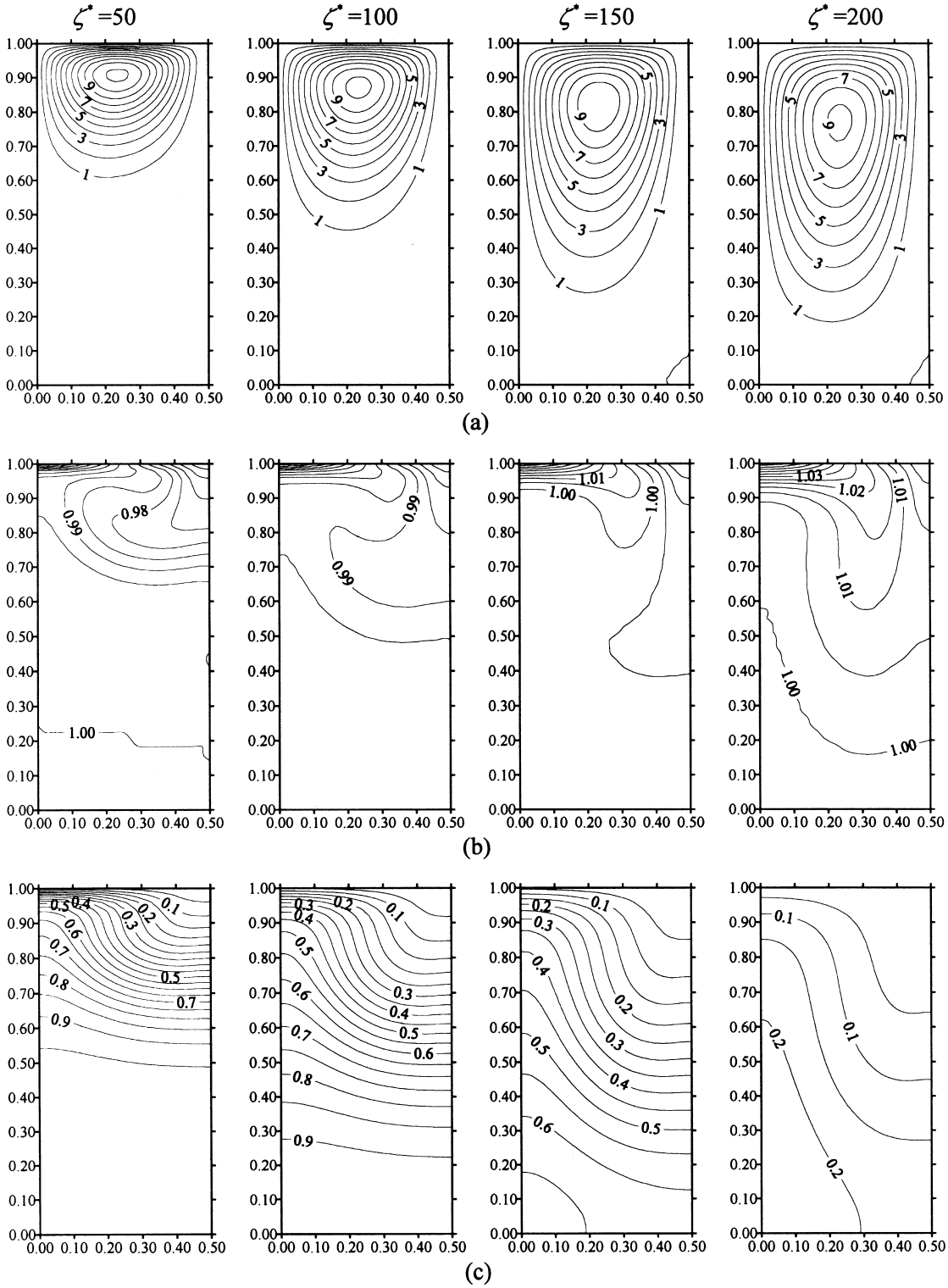

Fig. 4. The predicted stream function, temperature, and concentration contours of the solution in (ξ, η) domain at $\zeta^* = 50$, 100, 150, 200 with $Q_{in} = 5$, $Re = 10^4$, $Pr = 10$, $Sc = 10^4$, $Gr = 300$, $Bi = 100$, and $Bi_m = 300$.

this reason, the major clockwise vortex is formed in the upper portion of the domain and the center of circulation is closer to the free surface, away from the geometric center of the domain. Notably, the center of the recirculation zone moves slightly towards the hot center. The above transient behavior regarding the flow's development can be accounted for by the fact that under the high levels of the heating rate, an important temperature gradient takes place on the free surface. As a result, an intense flow develops. This also explains why very fine grids in the computational domain must be clustered near boundary surfaces to obtain reliable and accurate results. Conversely, on the bottom wall, the temperature gradients are milder and the fluid temperature near the left side of bottom surface is higher than that of the right side. Meanwhile, an intense surface flow develops, which transfers more energy by convection and adds momentum to the bulk fluid region along the solid wall. The direction of heat transfer by conduction is from the free surface to the interior region, because of the heat absorption at the free surface. The isotherms near the wall are almost distorted. Near the left symmetric surface of the domain, the direction of heat transfer by convection is opposite to the direction of heat conduction. The isotherms are nearly parallel to the free surface or, while thermocapillary flow is strong, even convex; this signifies a competition between the heat convection and conduction in the flow field. Regarding the time evolution of the heat and mass transfer process, this intense convection tends to transfer more heat deep into the interior region and the energy is transferred from the surface to the interior region by conduction. According to our results, the fluid temperature increases steadily with time, and the evaporation of solvent and heat convection from the free surface to ambient air tend to decrease the energy gain near the surface. These effects make the temperature field uniform within the fluid, particularly, on the free surface, and explain the diminution of the flow's intensity near the free surface. During the heating process, the distribution of solvent concentration affects the quantities of drying rate. As assumed herein, the evaporation of solvent occurs only at the free surface; the mass concentration noticeably and monotonously decreases from the interior region to the free surface. As the thermocapillary flow develops, thermocapillary forces cause a shear force in the interior fluid. The concentration field is influenced by the convection. Larger mass concentration can be transferred by convection from the interior region to the surface near the left side of the domain. Near the right side region, there is a competition between mass transfer by convection and by diffusion. Then the concentration value along the free surface decreases with the increasing distance ξ. Therefore, the further decrease in concentration of the solvent is noticeable as the intensity of Marangoni convection increases. As the absorbed radiative energy by polymer solution is decreased, the surface temperature gradient becomes smaller. Marangoni convection is completely contingent on thermal gradients at free surface. The flow field effectively responds to the diminishing temperature gradient over the free surface; the intensity of thermocapillary flow induced by surface tension gradient decreases. Near the left symmetric surface of the domain, the convex isotherms are not shown. Near the upper right region, the concentration gradient perpendicular to the surface is less than that for the case of larger Q_{in}.

Fig. 5(a) shows the variation of surface height of polymer solution S with respect to time for various values of Q_{in} at $Re = 10^4$, $Pr = 10$, $Sc = 10^4$, $Gr = 300$, $Bi = 100$ and $Bi_m = 300$. As the absorbed radiative energy by polymer solution is larger, the temperature will increase faster, and the drying rate increases more at the early stage of the drying process. When the surface water content decreases, the drying rate drops, but the temperature of the solution still increases. Since the internal temperature of polymer solution is much larger for larger Q_{in}, the diffusion of water from the interior region would enhance the drying rate during the latter process. And less drying time is required for larger radiant energy input. Similar contours of stream function, temperature and concentration are obtained as external heat and/or mass transfer parameters vary. Since the temperature of the ambient environment is equal to the initial temperature of the polymer solution after starting the heating process, the external convective effect not only carries the water vapor away from the solution surface, but also serves as a heat sink. As the external heat convective parameter is increased, the surface temperature gradient becomes smaller and the strength of thermocapillary flow induced by surface tension gradient decreases. While larger external mass convective parameter is utilized, more absorbed energy is supported to solvent evaporation. Plots of stream function, temperature and concentration contours show the same features as the above figures, while Bi and Bi_m vary. Fig. 5(b) shows the transient behavior of the heat and mass transfer processes in a polymer solution for various values of Bi at $Q_{in} = 10$, $Re = 10^4$, $Pr = 10$, $Sc = 10^4$, $Gr = 300$ and $Bi_m = 300$. When Bi is higher, the energy taken away from the solution surface by external heat transfer is larger. The absorbed energy supported to solvent evaporation is smaller and then required drying time is larger. Thus, higher external convective heating may not increase the drying speed, while the temperature of the ambient environment is lower than the free surface temperature. Fig. 5(c) presents the results for a polymer solution with various values of convective mass transfer Biot number Bi_m at

$Q_{in} = 10$, $Re = 10^4$, $Pr = 10$, $Sc = 10^4$, $Gr = 300$ and $Bi = 100$. With regard to the drying mechanism of the polymer solution, it is found that the drying rate initially increases when the external mass transfer is applied. For higher values of Bi_m, the drying rate reaches a maximum since the external transfer coefficient is larger, and then it decreases because of insufficient energy input. During the early drying period, the water content at the surface is higher. The water evaporation rate of the polymer solution is independent of the distribution of water content, and the drying rate is controlled by the external heating conditions. This is the so-called constant rate period. The water content near the surface decreases more with higher Bi_m. After the constant rate period, the drying rate drops and the temperature increases rapidly. Since the drying rate is dominated by the distribution of water, besides the diffusion of solvent, thermocapillary flow takes the solvent from the interior region to the free surface. Due to the higher external mass transfer, the drying rate increases much more at a higher value of Bi_m. Therefore, higher external mass convection can improve the

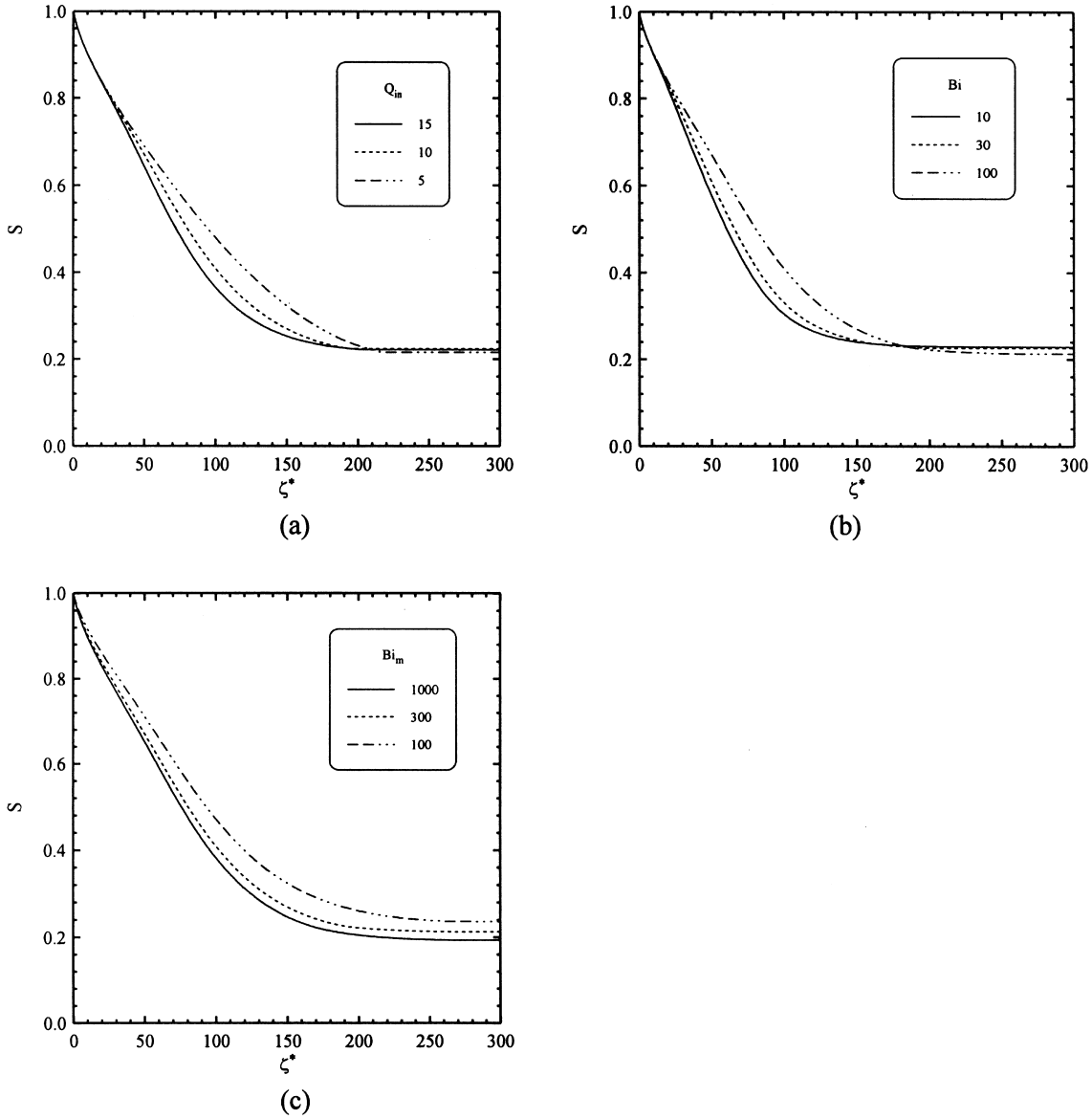

Fig. 5. Variations of solution height with respect to time: (a) at various radiant heat input, (b) at various values of Bi, and (c) at various values of Bi_m.

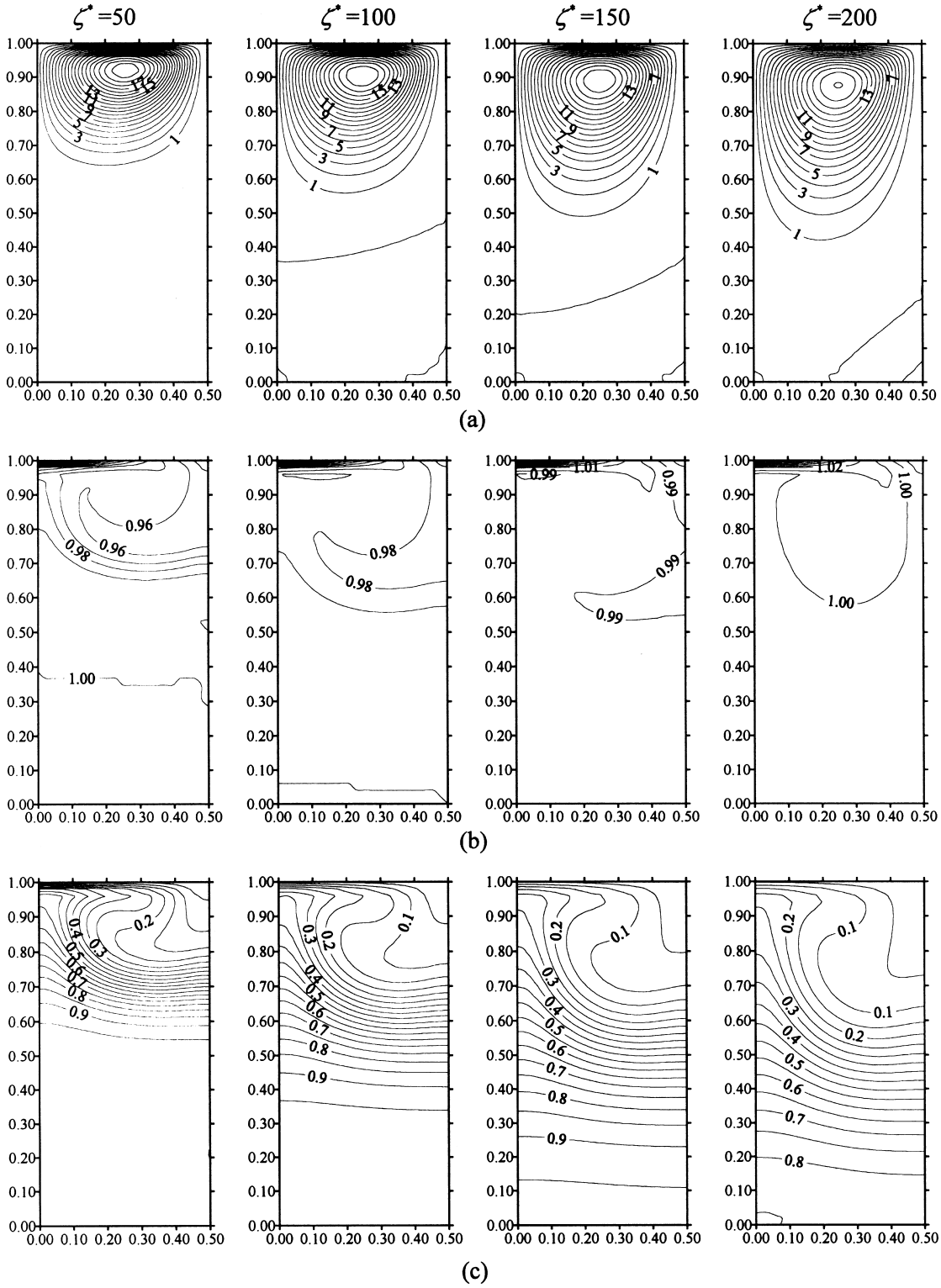

Fig. 6. The predicted stream function, temperature, and concentration contours of the solution in (ξ, η) domain at $\zeta^* = 50$, 100, 150, 200 with $Q_{in} = 10$, $Re = 5 \times 10^3$, $Pr = 10$, $Sc = 10^4$, $Gr = 300$, $Bi = 100$, and $Bi_m = 300$.

drying speed. From the results shown in the work of Chen and Lin [6], it is shown that a higher mass convective coefficient cannot definitely reduce the required drying time. However, while we consider the convective effect inside the solution, the water content near the bottom of the polymer solution is not only transferred towards the surface by diffusion but also by convection. Thus, the water can recover near the upper region, and the drying rate is larger for a higher value of Bi_m.

Fig. 6 shows the transient patterns of streamline, isotherm and iso-concentration lines for solution drying at $Q_{in} = 10$, $Re = 5 \times 10^3$, $Pr = 10$, $Sc = 10^4$, $Gr = 300$, $Bi_m = 300$ and $Bi = 100$. Compared to Fig. 3, it is noticed that the strength of thermocapillary flow induced by surface tension gradient increases as surface tension Reynolds number increases, and thermocapillary convection significantly affects the isotherm patterns near the free surface. When surface tension Reynolds number is smaller, the isotherm patterns are governed by conduction and, consequently, thermocapillary convection plays a minor role. Fur-

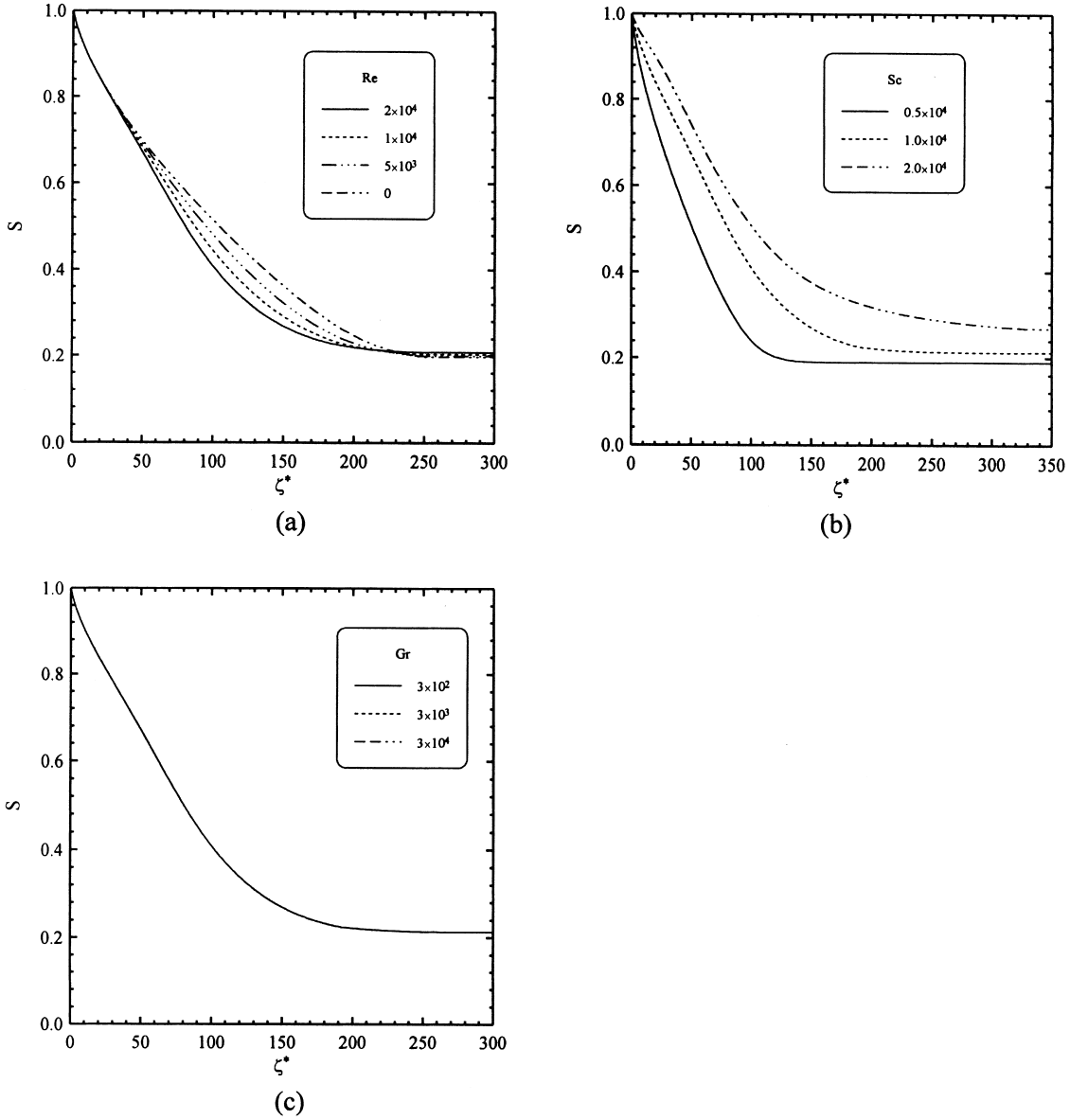

Fig. 7. Variations of solution height with respect to time: (a) at various values of *Re*, (b) at various values of *Sc*, and (c) at various values of *Gr*.

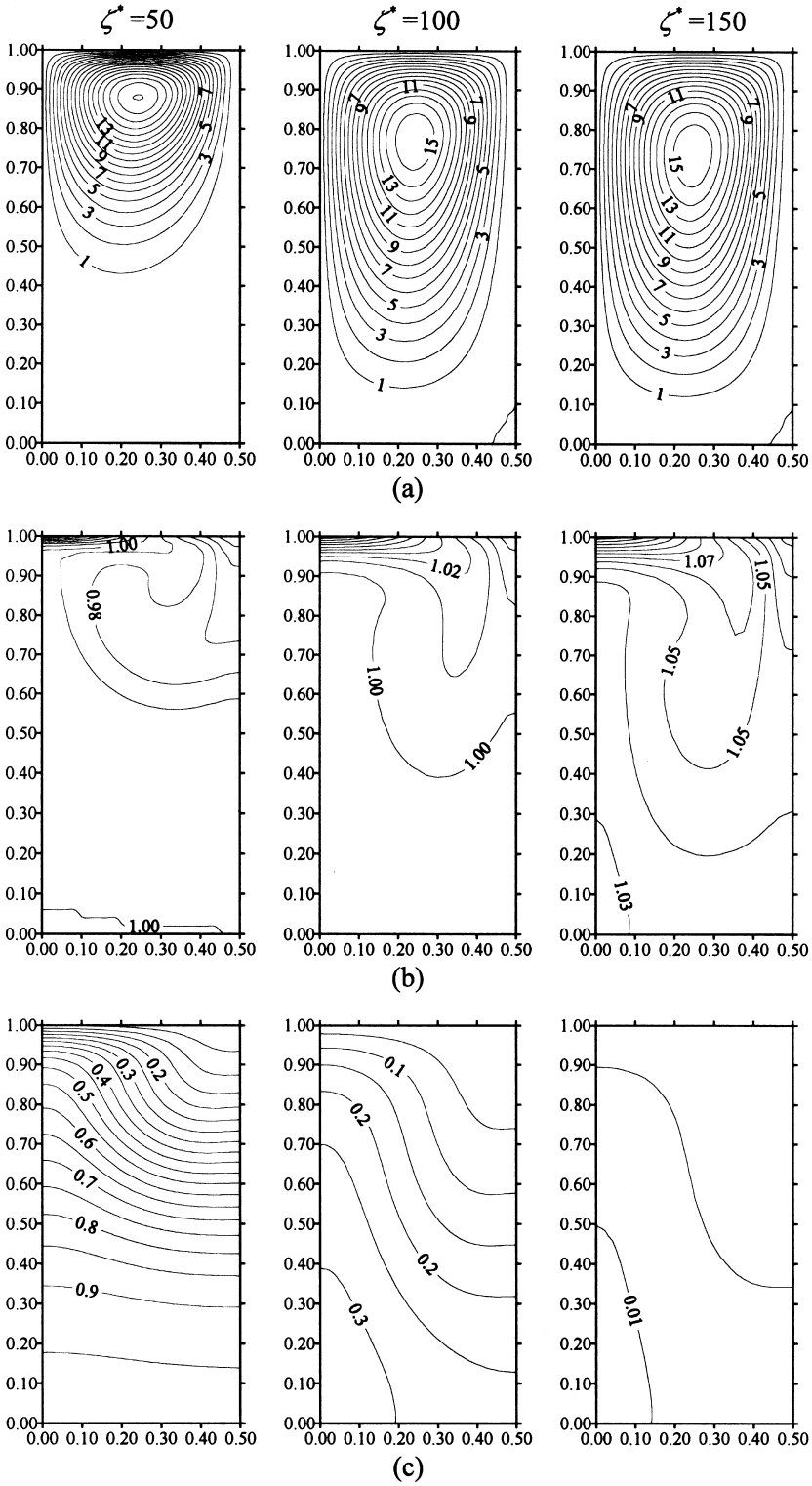

Fig. 8. The predicted stream function, temperature, and concentration contours of the solution in (ξ, η) domain at $\zeta^* = 50$, 100, 150 with $Q_{in} = 10$, $Re = 10^4$, $Pr = 10$, $Sc = 5 \times 10^3$, $Gr = 300$, $Bi = 100$, and $Bi_m = 300$.

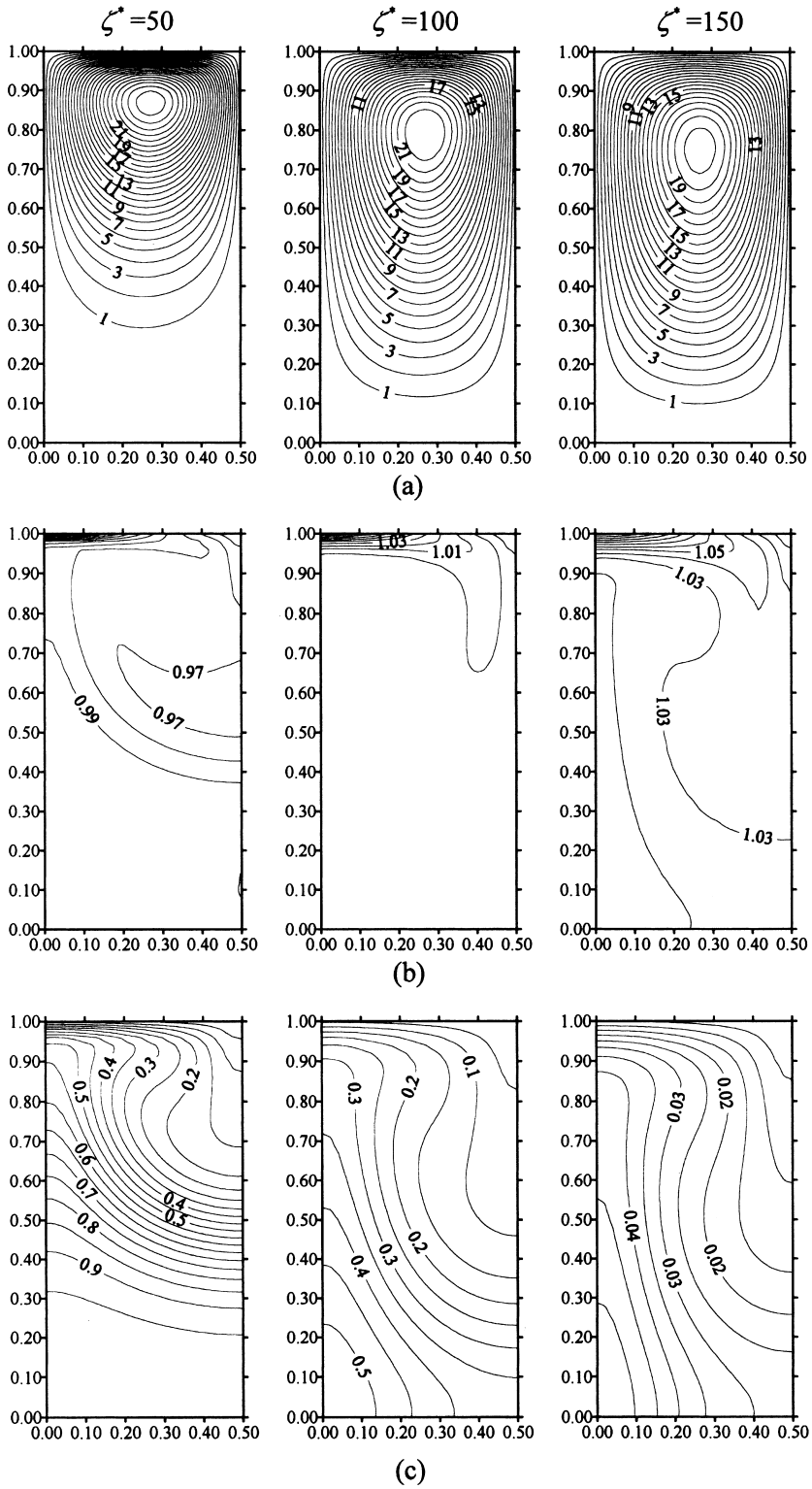

Fig. 9. The predicted stream function, temperature, and concentration contours of the solution in (ξ, η) domain at $\zeta^* = 50$, 100, 150 with $Q_{in} = 10$, $Re = 10^4$, $Pr = 10$, $Sc = 10^4$, $Gr = 300$, $Bi = 100$, and $Bi_m = 300$, while the side walls are symmetric.

thermore, the concentration field changes significantly for larger surface tension Reynolds number. More closely examining Fig. 7(a) reveals the effects of various surface tension Reynolds number on drying characteristics at $Q_{in} = 10$, $Pr = 10$, $Sc = 10^4$, $Gr = 300$, $Bi_m = 300$ and $Bi = 100$. Thermocapillary flow transfers more water content from the interior region to the free surface. Because of the recovery of water near the solution surface, the time required to complete the drying process is shorter as surface tension Reynolds number increases. For $Re = 0$, the effects of thermocapillary flows on the drying characteristics are not considered, the mechanism of mass transfer in solution is mass diffusion only and the drying rate is considerably decreased.

Prandtl number shows the relative importance of diffusion of vorticity to that of heat. From the transient behaviors of isotherm lines, the temperature difference inside the solution is unclear and the flow pattern of the liquid is similar to the variations of Pr. Thus, the discrepancy of the drying rate with the variations of Pr is not manifest. To examine the effect of Schmidt number, Sc, Fig. 8 shows transient development of the flow, temperature and concentration fields obtained for solution drying at $Q_{in} = 10$, $Re = 10^4$, $Pr = 10$, $Sc = 5 \times 10^3$, $Gr = 300$, $Bi_m = 300$ and $Bi = 100$. Corresponding results are listed from left to right for $\zeta^* = 50$, 100, and 150, respectively. The Schmidt number is the ratio of the momentum and mass diffusivities. While Sc is smaller, the ability of solvent mass diffusion is stronger. After initiating the heating process, the flow direction is clockwise in the domain and the solution flows downward along the side wall and upward along the symmetric surface. Then, the mass concentration can be transferred by convection from the interior region to the surface near the left side of the domain. Near the right side region, competition occurs between mass transfer by convection and by diffusion. More solvent can diffuse from the interior region to the surface as Sc decreases. This maintains a higher solvent concentration difference between the free surface and ambient environment. Fig. 7(b) presents the results of drying at various values of Schmidt number for $Q_{in} = 10$, $Re = 10^4$, $Pr = 10$, $Gr = 300$, $Bi_m = 300$ and $Bi = 100$. Decrease in Sc causes the external mass transfer to become larger; the drying rate is faster as well. Furthermore, The transient behavior remains quite similar features of stream function, temperature and concentration contours to that corresponding to the cases of various Gr. This study also examines the effect of various values of Grashof number Gr on the drying characteristics at $Q_{in} = 10$, $Re = 10^4$, $Pr = 10$, $Sc = 10^4$, $Bi_m = 300$ and $Bi = 100$, as shown in Fig. 7(c). The strength in the flow pattern increases with an increase of Gr and thus increases the convective transport. The mass concentration transferred from the interior region to the free surface increases more as Gr becomes larger. This is due to a similar reason as that mentioned in the last case. From the transient patterns of isotherm lines, the temperature difference inside the solution is not distinct, and the effect of buoyancy force on flow field is insignificant. Thus, the difference in drying rate is negligible with the variations of Gr. Similarly, the concentration variation in the direction of ξ inside the solution is small, the difference in drying rate can also be neglected with the variations of Gr_m.

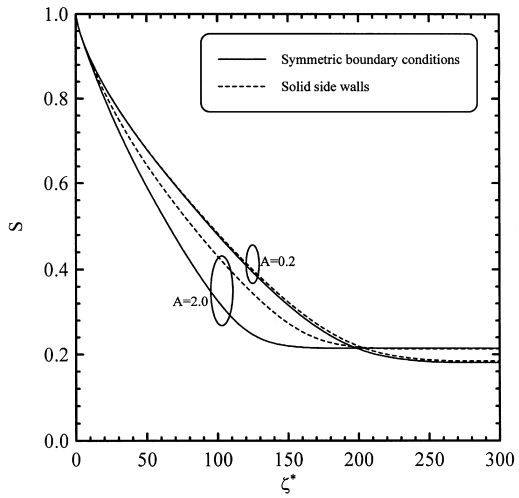

Fig. 10. Variations of solution height with respect to time at different hydrodynamic boundary conditions.

In the above results, effects of the various radiation input, external convective parameters, and important physical properties of solutions on drying characteristics are investigated in terms of flow, thermal and concentration fields, and drying rate for the case of aspect ratio, A, equal to 2.0. Similar results are obtained as aspect ratio is 0.2. Fig. 9 illustrates the streamlines, isothermal lines, and iso-concentration lines for $Q_{in} = 10$, $Re = 10^4$, $Pr = 10$, $Sc = 10^4$, $Gr = 300$, $Bi_m = 300$ and $Bi = 100$ at different hydrodynamic boundary condition, i.e., the symmetric side condition. In the present study, two different kinds of hydrodynamic boundary conditions are used, a solid wall at the right side of the computational domain or symmetric boundary conditions at the right side. The fluid immediately adjacent to the solid wall is at rest, relative to the wall. As the thermocapillary convection flow develops, the fluid rises along the left symmetric surface and sinks along the right surface of the domain. Then the flow velocity decreases as the fluid flows along the solid wall. Fig. 10 shows the effects of various hydrodynamic boundary conditions on drying rate at $Q_{in} = 10$, $Re = 10^4$, $Pr = 10$, $Sc = 10^4$, $Gr = 300$, $Bi_m = 300$ and $Bi = 100$. For the case of

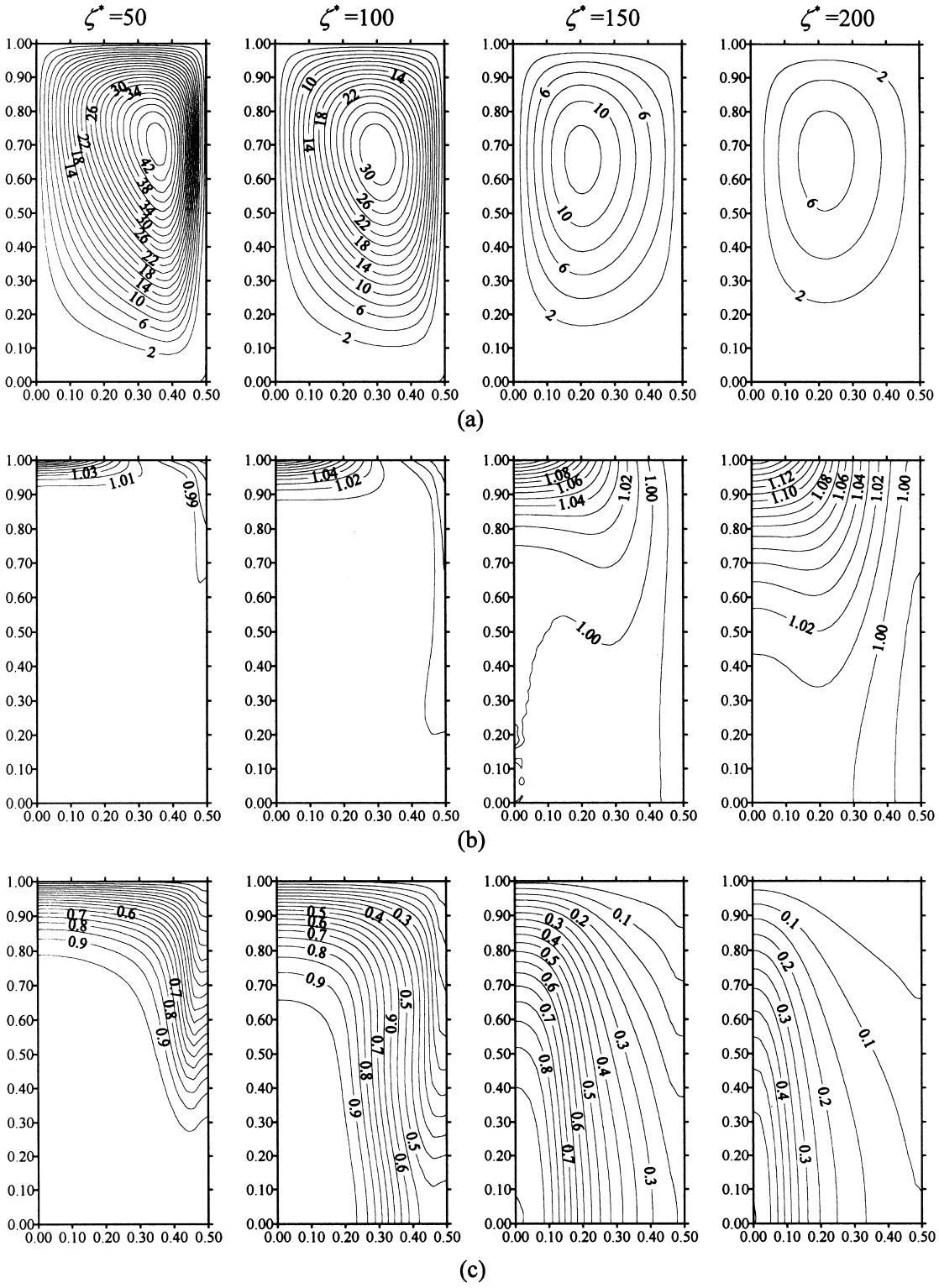

Fig. 11. The predicted stream function, temperature, and concentration contours of the solution in (ξ, η) domain at $\zeta^* = 50$, 100, 150, 200 with $Q_{in} = 10$, $Re = 10^4$, $Pr = 10$, $Sc = 10^4$, $Gr = 300$, $Bi = 100$, $Bi_m = 300$, and $A = 0.2$, while the side walls are solid.

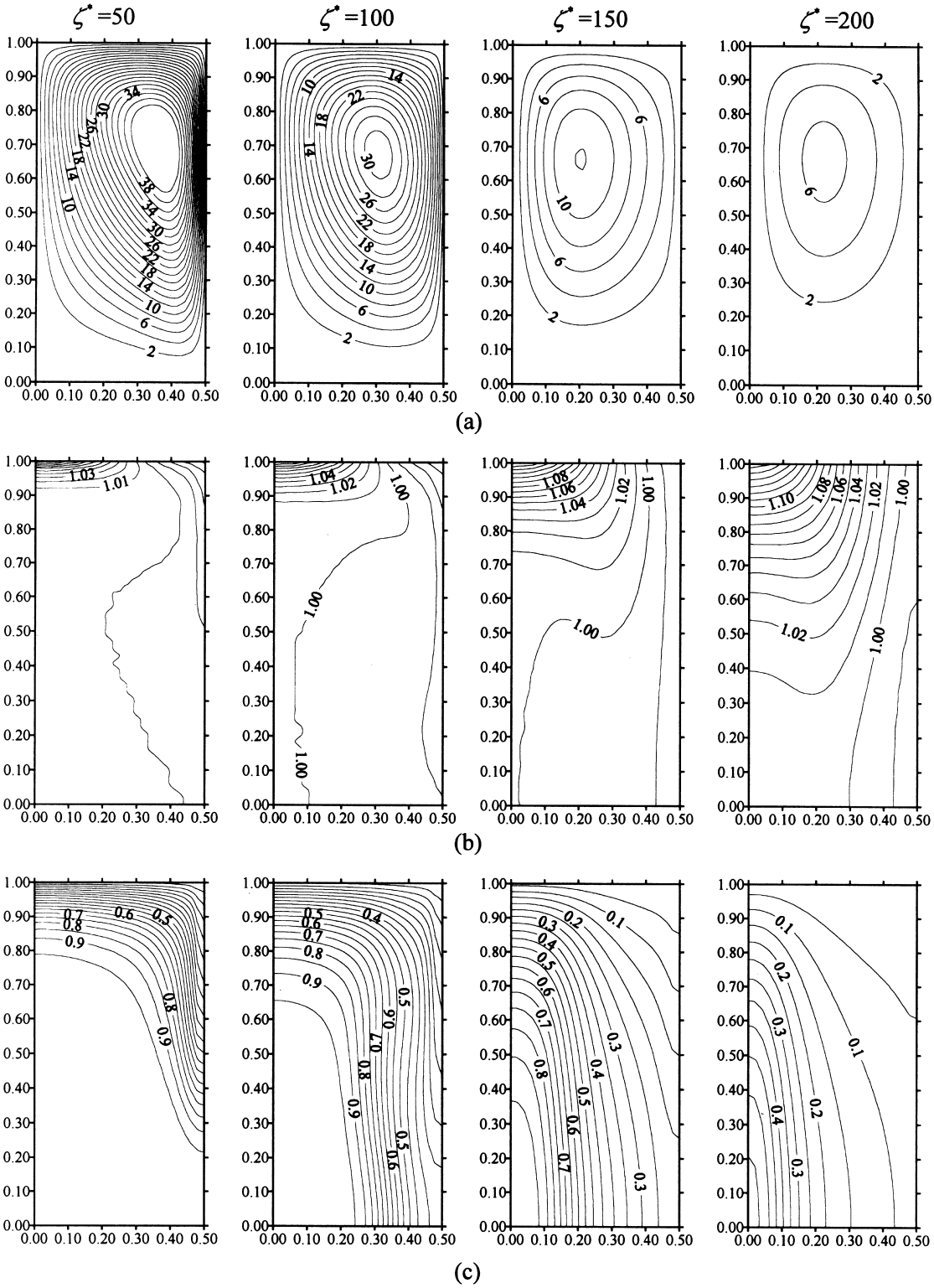

Fig. 12. The predicted stream function, temperature, and concentration contours of the solution in (ξ, η) domain at $\zeta^* = 50$, 100, 150, 200 with $Q_{in} = 10$, $Re = 10^4$, $Pr = 10$, $Sc = 10^4$, $Gr = 300$, $Bi = 100$, $Bi_m = 300$, and $A = 0.2$, while the side walls are symmetric.

$A = 2.0$, less mass concentration can transfer by convection from the interior region to the surface near the left side of the domain for a solution film with a solid side wall than that with symmetric side conditions. Thus, the drying rate is considerably decreased. While for the case of $A = 0.2$, we find that the influence of the boundary layer effect at the right solid wall on flow field is slight. Thus, the difference in drying rates between these cases is not distinct. Figs. 11 and 12 show the streamlines, isothermal lines, and iso-concentration lines for $Q_{in} = 10$, $Re = 10^4$, $Pr = 10$, $Sc = 10^4$, $Gr = 300$, $Bi_m = 300$, $Bi = 100$ and $A = 0.2$ at different hydrodynamic boundary conditions. It is found that the effect of the boundary layer on flow patterns is not significant. The local solution viscosity is increased as the water content is decreased. As the drying process proceeds, the viscosity of the solution near the surface grows larger than that near the bottom of the region. Thus, the intensity of thermocapillary flows decreases, and the velocity decreases for the case of small aspect ratio.

5. Conclusions

This study investigated the transient behavior of two-dimensional heat and mass transfer in polymer solutions under radiant heat. The problem is numerically studied using standard finite-difference techniques in the limit of infinitely small capillary number. The effects of various radiation input, external convection parameters, and important physical properties of solutions on heat and mass transfer processes are discussed in detail. According to the numerical results, the amount of radiant energy absorbed in the solution layer significantly influences the drying rate. In addition, external transfer parameters significantly affect drying characteristics. The drying rate decreases by using the cool external air flow as Bi increases. At larger value of Bi_m, the air flow can remove more solvent evaporated from the solution surface and thus, the drying rate is higher. It is also shown that forces driven by the surface tension has a crucial impact on the drying rate. At higher surface tension Reynolds number, thermocapillary flow carries more water content from the interior region to the free surface and leads to a shorter time for solution drying. The solvent near the surface is more concentrated owing to higher Sc, resulting in a higher drying rate. It is also worthy to point out that the effects of Pr, Gr and Gr_m on drying characteristics are negligible. In the case of a solution film with the symmetric side walls, removing the solid wall effect reduces the required drying time.

Acknowledgements

The authors would like to thank the National Science Council of the Republic of China for financially supporting this research under Contract No. NSC 86-2612-E-009-003.

References

[1] M. Okazaki, K. Shioda, K. Masuda, R. Toei, Drying mechanism of coated film of polymer solution, Journal of Chemical Engineering of Japan 7 (2) (1974) 99–105.
[2] Y. Sano, Drying of polymer solution, Drying Technology 10 (3) (1992) 591–622.
[3] J.S. Vrentas, C.M. Vrentas, Drying of solvent-coated polymer films, Journal of Polymer Science B: Polymer Physics 32 (1994) 187–194.
[4] B. Guerrier, C. Bouchard, C. Allain, C. Benard, Drying kinetics of polymer films, American Institute of Chemical Engineers Journal 44 (4) (1998) 791–798.
[5] M. Nishimura, M. Kuraishi, Y. Bando, Effect of internal heating on infrared drying of coated films, Heat Transfer — Japanese Research 12 (1983) 59–71.
[6] J.J. Chen, J.D. Lin, Simultaneous heat and mass transfer in polymer solutions exposed to intermittent infrared radiation heating, Numerical Heat Transfer A 33 (1998) 851–873.
[7] R. Dhib, A.D. Broadbent, N. Therien, Modeling and simulation of the drying of thin sheets in a continuous infrared dryer, Canadian Journal of Chemical Engineering 72 (1994) 894–905.
[8] H.D. Kuang, J. Thilbault, R. Chen, B.P.A. Grandjean, Pilot scale investigation of infrared drying of paper, Tappi Journal 78 (7) (1995) 129–137.
[9] A. Hashimoto, K. Hirota, T. Honda, M. Shimiza, A. Watanabe, Factors influencing constant drying rate of wet granular bed irradiated by infrared radiation, Journal of Chemical Engineering of Japan 24 (6) (1991) 748–755.
[10] E.B. Gutoff, E.D. Cohen, G.I. Kheboian, Coating and Drying Defects, Wiley, New York, 1995.
[11] M.J. Tan, S.G. Bankoff, S.H. Davis, Steady thermocapillary flows of thin liquid layers. Part I: theory, Physics of Fluids A 2 (3) (1990) 313–321.
[12] D.L. Hitt, M.K. Smith, Radiation-driven thermocapillary flows in optically thick liquid films, Physics of Fluids A 5 (11) (1993) 2624–2632.
[13] J.R.A. Pearson, On convection cells induced by surface tension, Journal of Fluid Mechanics 4 (1958) 489–500.
[14] H.B. Hadid, B. Roux, Buoyancy- and thermocapillary-driven flows in differentially heated cavities for low-Prandtl-number fluids, Journal of Fluid Mechanics 235 (1992) 1–36.
[15] M. Hozawa, M. Inoue, J. Sato, T. Tsukada, N. Imaishi, Marangoni convection during steam absorption into aqueous LiBr solution with surfactant, Journal of Chemical Engineering of Japan 24 (2) (1991) 209–214.
[16] I. Ahmed, K.S. Ball, Spectral simulation of thermocapillary convection with deformable free surface using

boundary-fitted coordinates, Numerical Heat Transfer B 32 (1997) 127–149.

[17] J.J. Chen, Analysis of heat and mass transfer in drying process of polymer solutions using infrared radiative heating, Ph.D. thesis, National Chiao Tung University, Hsinchu, Taiwan, 1999.

[18] J.F. Thompson, F.C. Thames, C.W. Mastin, Automatic numerical generation of body fitted curvilinear coordinate system for field containing any number of arbitrary two-dimensional bodies, Journal of Computational Physics 15 (1974) 299–319.

[19] T.P. Blomstrom, Vinyl alcohol polymers, in: H.F. Mark, D.F. Othmer, C.G. Overberger (Eds.), Encyclopedia of Chemical Technology, vol. 17, 1978, p. 173.

[20] J.P. Holman, Heat Transfer, McGraw-Hill, New York, 1989.